



UNIVERSITY OF LEEDS

This is a repository copy of *Pre-failure instability of sand under dilatancy rate controlled conditions*.

White Rose Research Online URL for this paper:
<http://eprints.whiterose.ac.uk/109390/>

Version: Accepted Version

Article:

Chu, J, Wanatowski, D, Loke, WL et al. (1 more author) (2015) Pre-failure instability of sand under dilatancy rate controlled conditions. *Soils and Foundations*, 55 (2). pp. 414-424. ISSN 0038-0806

<https://doi.org/10.1016/j.sandf.2015.02.015>

For example: © 2015. This manuscript version is made available under the CC-BY-NC-ND 4.0 license <http://creativecommons.org/licenses/by-nc-nd/4.0/>

Reuse

Items deposited in White Rose Research Online are protected by copyright, with all rights reserved unless indicated otherwise. They may be downloaded and/or printed for private study, or other acts as permitted by national copyright laws. The publisher or other rights holders may allow further reproduction and re-use of the full text version. This is indicated by the licence information on the White Rose Research Online record for the item.

Takedown

If you consider content in White Rose Research Online to be in breach of UK law, please notify us by emailing eprints@whiterose.ac.uk including the URL of the record and the reason for the withdrawal request.



eprints@whiterose.ac.uk
<https://eprints.whiterose.ac.uk/>

Pre-failure instability of sand under dilatancy rate controlled conditions

J. Chu¹, D. Wanatowski^{2*}, W.L. Loke³ and W.K. Leong⁴

¹Professor, Iowa State University, Department of Civil, Construction & Environmental Engineering, 328 Town Engineering Building, Ames, IA 50011, US.

Email: jchu@iastate.edu

^{2*}Associate Professor, Department of Civil Engineering, Faculty of Science and Engineering, The University of Nottingham, Ningbo, China.

Email: d.wanatowski@nottingham.edu.cn (Corresponding author).

³Project Manager/Offshore Engineer, Braemar Technical Services (Offshore) Pte Ltd, Singapore

Email: Ashley.loke@braemar

⁴Senior Geotechnical Engineer, Houston, Texas, US.

Email: leong.wingkai@arup.com

Abstract: Experimental results are presented in this paper to show that a runaway type of pre-failure instability can occur for sand under dilatancy rate controlled conditions when an appropriate strain increment ratio, $d\varepsilon_v/d\varepsilon_1$, is imposed. This type of instability is similar to the runaway type of instability observed for very loose sand under undrained conditions. Whether a soil element will undergo pre-failure instability depends on the difference between the strain increment ratio of the soil obtained from drained test, under a specified effective confining pressure, $(d\varepsilon_v/d\varepsilon_1)_s$, and the strain increment ratio imposed during the test, $(d\varepsilon_v/d\varepsilon_1)_i$, rather than the absolute magnitude of $(d\varepsilon_v/d\varepsilon_1)_s$. Based on the experimental data obtained in this study it was found that an instability line can be determined from a series of strain path tests conducted at different effective confining pressures but with the same $d\varepsilon_v/d\varepsilon_1$ by joining the peak points of the effective stress paths to the origin in the q - p' stress space. This line is similar to the instability line obtained from undrained tests on loose sand. The instability tests under dilatancy rate controlled conditions indicate that the stress ratio at the onset of instability obtained in the instability tests coincide with the peak stress ratio line. This suggests that the peak stress line can be used to predict the onset of instability under dilatancy rate controlled conditions in the same way as the use of instability line to predict the onset of instability under undrained conditions.

KEYWORDS: liquefaction, sands, laboratory testing, shear strength.

INTRODUCTION

Failure of geotechnical structures can be initiated by instability of soil. The term instability used in this paper refers to a behaviour in which large plastic strains are generated rapidly due to the inability of a soil element to sustain a given load or stress. Instability normally takes place when the stress state of a soil element satisfies a failure criterion, as in the conventional stability analysis. However, instability may also occur prior to attaining the failure stress state. A typical example is static liquefaction which occurs before the effective stress path reaches the failure line (which is also the steady state line for loose sand). So far, this so called pre-failure instability has been observed mainly for saturated loose sand under undrained conditions (e.g. Lade & Pradel 1990; Lade 1993; Leong et al. 2000, Yang 2002, Wanatowski & Chu 2007, 2012, Andrade 2009). However, the undrained condition may not be necessary. There are failure cases that occurred under drained or other than undrained conditions (e.g. Torrey & Weaver, 1984; Eckersley, 1990; Olson et al., 2000; Kokusho 2003; Sento et al., 2004). Failure mechanisms related to the re-distribution of void ratio within a globally undrained sand layer (Fig. 1a) or spreading of excess pore water pressure with global volume changes along a slope (Fig. 1b) have been suggested by the U.S. National Research Council (NRC 1985). Adalier & Elgamal (2002) also observed from a series of centrifuge tests that there is a potential strength loss in dense sand as a result of pore water migration into the dense zone from the adjacent loose zone in the ground. This further indicates that flow slides can take place under other than undrained conditions. These, other than undrained or the so-called non-undrained conditions (Chu et al. 1992), have been simulated in the laboratory by the use of a strain path testing method (Chu & Lo 1991), in which the strain increment ratio, $d\varepsilon_v/d\varepsilon_1$, imposed to a specimen, is controlled. When $d\varepsilon_v/d\varepsilon_1 > 0$, the soil specimen compresses and when $d\varepsilon_v/d\varepsilon_1 < 0$, the specimen dilates. An undrained test is only a special case when $d\varepsilon_v/d\varepsilon_1 = 0$. The strain path method also provides a better simulation of the field situations, where a soil element will normally experience both volume change and pore water pressure change simultaneously and fully drained or undrained conditions are only exceptional cases. However, the use of strain path testing

method to study soil behaviour is uncommon (Topolnicki et al. 1990; Chu et al. 1992, 1993; Vaid & Eliadorani 1998, Lancelot et al. 2004; Sivathayalan & Logeswaran 2007; Wanatowski et al. 2008, Wanatowski and Chu 2011).

The possibility of dilating behaviour of soil masses prior to slope collapse has also been reported in several case studies. For example, Been et al. (1987) argued that the Nerlerk berm failure case might have occurred for dilatant sand which state lies below the steady state line. Several other cases of flowslide in dilatant sand have been presented by Been et al. (1988). Fleming et al. (1989) also reported that the Salmon Creek landslide in Marin Country, California, exhibited dominantly dilative transformation from solid landslide to liquid debris flow. Although some explanations to the causes of this and other failures have been proposed (Schofield 1980, Been et al. 1988; Hadala & Torrey 1989), the instability mechanisms of dilative sand have not been well established. Furthermore, a method to predict such failures has not been proposed yet.

The objective of this paper is to study the pre-failure instability of sand in strain path testing under dilatancy rate controlled conditions. The results of the strain path tests conducted on medium loose to medium dense sand are presented. Factors affecting the occurrence of pre-failure instability under dilatancy rate controlled conditions are analysed. The practical implications of the study are also discussed.

MATERIAL TESTED AND TESTING PROCEDURES

A marine-dredged sand was used for this experimental study. The basic properties of the sand are given in Table 1. All the specimens were prepared by pluviating sand into water. For saturation, all the specimens were flushed with de-aired water from the bottom to the top for 60 minutes under a water head of about 0.5 m. After that a back pressure of 400 kPa was applied. The Skempton's pore water pressure parameter (B-value) greater than 0.96 was obtained for all the specimens. A liquid rubber technique (Lo et al. 1989) was adopted to reduce the bedding and membrane penetration errors. The specimens used were 200 mm in height and 100 mm in diameter.

All the specimens were isotropically consolidated. Shearing in all the tests was carried out using a strain path method with $d\varepsilon_v/d\varepsilon_1 = \text{const}$ (Chu & Lo 1991). In the strain path method, when $d\varepsilon_v/d\varepsilon_1 > 0$, the soil element is in compression and water flows out of the specimen. When $d\varepsilon_v/d\varepsilon_1 < 0$, the soil element is in dilation and water flows into the specimen. An undrained test, with $d\varepsilon_v/d\varepsilon_1 = 0$, is only a special case of the $d\varepsilon_v/d\varepsilon_1 = \text{const}$ test. Since in a strain path test the volumetric change of the specimen is controlled, a change in pore water pressure occurs. This change in pore water pressure leads to a change in effective confining stress.

In this study a $d\varepsilon_v/d\varepsilon_1 = \text{const}$ strain path was imposed on a soil specimen by controlling the volume change of the specimen via the Digital Pressure/Volume Controller (DPVC) in accordance with the measured axial deformation. The DPVC was used to control the volume of water flowing out (for contractive strain paths) or flowing into the specimen (for dilative strain paths) at a desired volume change rate. The applied volume change could be controlled with accuracy of 0.1% measured value with $\pm 20\text{mm}^3$ backlash.

All the tests were computer controlled. The control loop consisted of the following steps:

- (1) compute the axial strain from the deformation measured by the pair of internal LVDTs,
- (2) compute ε_v and hence the volume change to be imposed by the DPVC according to the required $d\varepsilon_v/d\varepsilon_1$,
- (3) send signal to DPVC to target the required volume change,
- (4) read all transducers, plot the strain path followed and the effective stress state, record stress-strain parameters and return to step 1.

The continuous plotting of the actual strain path and the effective stress state followed at step (4) enabled the detection of any out of control. Satisfactory control was achieved for all the tests.

Two types of strain path tests were carried out in this study. The first type, a deformation-controlled (DC) strain path test was carried out with either negative or positive strain increment ratio using a constant deformation rate of 0.05 mm/min. The second type, a load-controlled (LC)

strain path test (so-called strain path instability test) was carried out with a negative strain increment ratio and with the deviator (vertical) load kept constant. In both types of tests the vertical load and deformation could be successfully controlled via a digital hydraulic force actuator mounted at the bottom of a loading frame to apply axial load. The actuator was controlled by a computer via a digital load/displacement control box. The control box adjusted the movement of the base pedestal to achieve a desired rate of load or rate of displacement so that the triaxial apparatus could be used under either deformation-controlled or load-controlled loading mode.

TESTING ARRANGEMENT

The experiments were carried out using a fully automated triaxial testing system. A digital pressure volume controller (DPVC) with a remote feedback module was used to control the axial load via a hydraulic actuator. Another DPVC was used to control the confining stress. A third DPVC was used to control the back pressure via the base of the specimen and measure the volume change at the same time. Two submersible linear variable differential transformers (LVDTs) were attached onto the specimen for the measurement of axial strain up to approximately 4%. An external LVDT of 50 mm travel was mounted directly on top of the triaxial chamber for the purpose of measuring large strains. To minimise the bedding errors and achieve as uniform strain distribution as possible during the test, free-ends with enlarged platens were used (Rowe & Barden 1964). The pore water pressure at the top of the specimen was measured by a pressure transducer. For details of the testing arrangement see Chu & Leong (2001).

UNDRAINED BEHAVIOUR OF LOOSE AND DENSE SAND

The stress-strain behaviour of sand under undrained conditions is void ratio dependent and may vary from strain softening to strain hardening type. The type of behaviour obtained from an undrained triaxial test depends on the relation between the initial void ratio of the sand tested, e_0 , and the critical void ratio, e_{cr} , (Casagrande 1936) which sets the boundary between strain hardening

and strain softening behaviour of the sand under the given mean effective stress. Sometimes only a slight change in density can convert the behaviour of soil from strain hardening to strain softening.

The typical stress-strain behaviour of sand in an undrained triaxial test is presented in Fig. 2(a). It can be seen that for loose sand with $e_0 > e_{cr}$ (i.e. looser than critical void ratio) deviatoric stress reaches its peak and then decreases to an ultimate value with increasing axial strain. This type of behaviour is termed as the strain softening. When $e_0 = e_{cr}$, the deviatoric stress remains constant after the peak is attained, as shown in Fig. 2(a). Once the void ratio of the soil, e_0 , is smaller than, the critical void ratio, e_{cr} , the strain hardening behaviour is observed. Furthermore, the smaller the void ratio (i.e. the higher density), the stiffer stress-strain response is obtained, as shown in Fig. 2(a).

The corresponding effective stress paths of the stress-strain curves shown in Fig. 2(a) are plotted in Fig. 2(b) together with the critical state line (CSL) and the failure line (FL) obtained from drained triaxial tests on loose and dense sand, respectively. As shown in Fig. 2(b), in the undrained test on loose sand with $e_0 > e_{cr}$ the effective stress path increases gradually towards the peak state and then traces down towards the CSL showing flow or strain softening behaviour. The effective stress path of loose sand with $e_0 = e_{cr}$ also increases towards the peak state but then remains constant at the critical state line. For loose sand with $e_0 < e_{cr}$, the effective stress path of an undrained test increases towards the peak and then follows the CSL.

The effective stress path obtained from an undrained test on dense sand with e_0 much greater than e_{cr} is also shown in Fig. 2(b). It can be seen that for dense (i.e. dilative) sand, the effective stress path of a CIU test will increase monotonically and approach a constant stress ratio line (CSRL). In this case, the peak and the critical state cannot be determined because the specimen exhibits strain hardening behaviour and the deviatoric stress increases with axial strain throughout the entire undrained shearing. Such stress hardening behaviour under undrained conditions is often referred to as non-flow.

INSTABILITY LINE FOR LOOSE SAND UNDER UNDRAINED CONDITIONS

It needs to be emphasised that if an undrained test is conducted on loose sand with $e_0 > e_{cr}$ under a load controlled loading condition the specimen will become unstable at the peak state. This behaviour has often been referred to as static liquefaction. However, if an undrained test is conducted on loose sand under a deformation controlled loading condition, static liquefaction or instability in the form of a sudden increase in axial strain rate will not occur, e.g., test on loose sand with $e_0 > e_{cr}$ in Fig. 2. In this case, strain softening in the form of a reduction in the deviatoric stress occurs instead (Chu & Leong 2001; Chu & Wanatowski 2009).

It has been established by Lade (1992) that instability occurs when the stress ratio at the onset of instability is above the instability line, which is defined as the line connecting the top of the effective stress paths of loose sand sheared under an undrained condition, as shown in Fig. 3. The zone between the instability line and the critical state line is called the zone of potential instability which specifies the instability condition for loose sand under undrained conditions (Lade 1992, 1993). Therefore, the instability line separates potentially unstable stress states from stable stress states. Lade (1992) explained that the stress state at which instability would occur corresponds to the top of the current yield surface which is slightly before, but very close to, the top of the undrained effective stress path. Therefore, the instability line can be determined experimentally by a line connecting the peak of a series of effective stress paths obtained from undrained tests. Other definitions similar to the instability line have also been given to specify the instability condition, such as the collapse surface by Sladen et al. (1985), the state boundary surface by Sasitharan et al. (1993), and or the flow liquefaction line by Yang (2002). However, the differences among the different definitions are small, as pointed out by Lade (1993) and Chu et al. (2003). The physical meanings behind the different interpretations are also essentially the same, i.e., to specify a yielding point where large plastic strains can develop (Chu et al. 2003).

BEHAVIOUR OF DENSE SAND UNDER DILATANCY RATE

CONTROLLED CONDITIONS

As shown in Fig. 2 strain softening does not usually occur for dense sand under undrained conditions. However, strain softening may occur if a dense sand specimen is sheared along a strain path with $d\varepsilon_v/d\varepsilon_1 < 0$ (Chu et al. 1992, Chu & Leong 2001, Wanatowski et al. 2008).

Typical behaviour of dense Changi sand under dilative strain path is presented in Fig. 4 where results of two tests SP10 and SP12 carried out with $d\varepsilon_v/d\varepsilon_1 = -0.67$ and $d\varepsilon_v/d\varepsilon_1 = 0$ (i.e undrained test) respectively, are compared. The specimens were isotropically consolidated to the mean effective stress $p_c' = 150$ kPa. The void ratios of the specimens in Tests SP10 and SP12 were 0.766 and 0.764, respectively, which corresponds to a medium dense state.

The stress-strain curves of the two tests are shown in Fig. 4(a). It can be seen that strain hardening behaviour was observed in undrained test SP12. However, strain softening behaviour, similar to that of loose sand under an undrained condition, was obtained from Test SP10 with dilative strain increment ratio $d\varepsilon_v/d\varepsilon_1 = -0.67$ imposed to the specimen.

The effective stress paths obtained from the two tests are shown in Fig. 4(b). The critical state line (CSL) and the failure line (FL) obtained from drained triaxial tests on loose and medium dense sand, respectively together with the constant stress ratio line (CSRL) obtained from undrained triaxial tests on medium dense sand (Chu et al. 2003) are also plotted in Fig. 4(b). It can be seen from Fig. 4(b) that the effective stress path of Test SP10 increases until the peak state and then reduces gradually along the failure line (FL) reaching the origin of the stress plane at the end of test. This behaviour resembles flow behaviour of loose sand under an undrained condition. The effective stress path of the undrained test SP12, on the other hand, increases monotonically and approach a constant stress ratio line (CSRL). In other words, strain hardening behaviour is observed. It is interesting to note that in the case of undrained test on medium dense sand, a peak state, the critical state and the failure state determined from drained tests are no longer obtainable.

The excess pore water pressures developed in the two tests are compared in Fig. 4(c). It can be seen that the pore water pressure in Test SP10 with $d\varepsilon_v/d\varepsilon_1 = -0.67$ imposed increased during the entire shearing stage. However, the pore water pressure in the undrained test SP12 with $d\varepsilon_v/d\varepsilon_1 = 0$ imposed, increased initially to the peak (i.e. Δu_{\max}) and then reduced gradually until the end of the test. As a result strain hardening was observed in Test SP12, as shown in Figs. 4(a) and (b).

It can also be noted from Fig. 4(c) that the excess pore water pressure developed in an undrained test is not the largest, as often assumed. The pore water generation for the undrained path is lower than that for a negative (dilative) strain path.

The tests results shown in Fig. 4 clearly demonstrate that stress-strain behaviour of granular soil sheared from the same initial conditions (i.e. void ratio and mean effective stress) can vary from strain softening to strain hardening. As established by Chu et al. (1992), whether a soil element will undergo strain hardening or softening depends on the relative magnitude of the strain increment ratio of the soil obtained from conventional drained test, $(d\varepsilon_v/d\varepsilon_1)_s$ and the strain increment ratio, $(d\varepsilon_v/d\varepsilon_1)_i$ imposed during the test. This means that a soil specimen undergoing contractive volumetric change can experience strain softening behaviour if the strain increment ratio imposed during the strain path test, $(d\varepsilon_v/d\varepsilon_1)_i$ is smaller (i.e. less compressive) than the strain increment ratio of the soil obtained from a conventional drained test, $(d\varepsilon_v/d\varepsilon_1)_s$. The conditions for the occurrence of strain-softening and strain-hardening as established by Chu et al. (1992) are presented in Inequalities (1a), (1b) and (1c) below:

$$(d\varepsilon_v/d\varepsilon_1)_i - (d\varepsilon_v/d\varepsilon_1)_s > 0 \text{ ----- hardening} \quad (1a)$$

$$(d\varepsilon_v/d\varepsilon_1)_i - (d\varepsilon_v/d\varepsilon_1)_s = 0 \text{ ----- perfectly plastic} \quad (1b)$$

$$(d\varepsilon_v/d\varepsilon_1)_i - (d\varepsilon_v/d\varepsilon_1)_s < 0 \text{ ----- softening} \quad (1c)$$

where $(d\varepsilon_v/d\varepsilon_1)_s$ = the strain increment ratio of the soil obtained from a conventional drained test and $(d\varepsilon_v/d\varepsilon_1)_i$ = the strain increment ratio imposed during a strain path test. For more details, see Chu et al. (1992) and Wanatowski et al. (2008).

INSTABILITY LINE FOR DENSE SAND UNDER DILATANCY RATE CONTROLLED CONDITIONS

As discussed earlier, the instability line for undrained conditions can be determined by joining the peak points of the effective undrained stress paths of loose sand. It was also shown in Fig. 4(b) that the effective stress path obtained from a dilative strain path test on medium dense sand is very similar to that of undrained test on loose sand. Therefore, a similar method to that under undrained conditions may also be used to determine a line by connecting the peak points of the effective stress paths. In this paper, such a line determined for dense sand under dilatancy-controlled conditions will be referred to as '*peak stress line*'.

Figure 5 shows the results of three strain path tests (SP09, SP10 and SP11) of $d\varepsilon_v/d\varepsilon_1 = -0.67$. The specimens were isotropically consolidated to mean effective stresses of 150 kPa, 300 kPa, and 500 kPa. The void ratios, e_c measured in tests SP09, SP10 and SP11 were 0.760, 0.766 and 0.763, respectively.

The stress-strain curves measured in the three tests are plotted in Fig. 5(a). It can be seen that strain softening behaviour was obtained for all three specimens. All the stress-strain curves reached the peak states (points A, B and C) at low level of the axial strain and then reduced gradually to very low deviatoric stresses.

The effective stress paths of the three tests are shown in Fig. 5(b). All the paths show similar strain softening behaviour, in which the peak stresses (A, B, and C) are initially reached and a unique failure envelope determined by drained tests is approached. As shown in Fig. 5(b), by joining the peak stresses A, B and C with the origin of the q-p' plane, a peak stress line with a slope of $\eta_p = 1.13$, can be established. From the stress-strain curves presented in Fig. 5(a), it can be seen clearly that strain softening and large plastic yielding occurred at points A, B and C for all the three tests. Therefore, points A, B and C define the yielding points for Tests SP09, SP10 and SP11, respectively.

The excess pore water pressures developed in the three tests are shown in Fig. 5(c). It can be noted that pore water pressures increase gradually in all the tests, which again is similar to the undrained behaviour of loose sand. It can also be seen from Fig. 5(c) that the excess pore water pressure increases with the initial confining stress.

Based on the experimental data shown in Fig. 5 it can be concluded that pre-failure strain softening can occur in a dilative strain path test in a way similar to that for loose sand under undrained conditions. From the study of instability behaviour of granular soils under undrained conditions, we know that the instability line is determined by joining the peak points of the undrained stress paths, which are very close to the top of the yield surface. Thus, the peak stress line obtained in Fig. 5(b) that specifies the yielding for tests conducted under dilatancy rate controlled conditions could also be defined as the instability line for pre-failure instability occurring under dilatancy-controlled conditions. The zone bounded by the peak stress line and the failure line could then define the zone of potential instability for medium dense sand under dilatancy rate controlled conditions.

From the experimental results presented above, it can be seen that the strain increment ratio affects the instability behaviour of sand. This is consistent with other experimental observations reported in the literature (Chu et al. 1993; Chu & Leong 2001; Vaid and Eliadorani 1998; Lancelot et al. 2004; Sivathayalan and Logeswaran 2007; Wanatowski & Chu 2011). It was shown that the more dilative the $d\varepsilon_v/d\varepsilon_l$ imposed to the specimen, the higher the tendency for instability to occur. This is because when a $d\varepsilon_v/d\varepsilon_l$ larger than the dilatancy ratio of the soil is imposed, the pore water pressure will increase. This in turn leads to a decrease in effective confining stress and causes instability when the instability line is crossed. This means the location of instability line depends on dilatancy rate imposed to the specimen and the instability zone must therefore be determined based on the peak stress line and the failure line defined for specific dilatancy rate and void ratio. Once instability lines for different dilatancy rates and void ratios are determined, the instability boundary

on the e_c versus $(d\varepsilon_v/d\varepsilon_1)_i$ plane can be determined (Wanatowski et al. 2008; Wanatowski and Chu 2011).

PRE-FAILURE INSTABILITY OF SAND UNDER DILATANCY RATE CONTROLLED CONDITIONS

Several load-controlled strain path tests were carried out in this study to verify whether the peak state line determined from dilative strain path tests under deformation-controlled loading conditions can be used to predict the occurrence of pre-failure instability under load-controlled loading conditions.

Firstly, an instability test IST01 was conducted on medium dense sand to verify whether pre-failure instability can occur under load-controlled loading mode. The effective stress path obtained from Test IST01 is plotted in Fig. 6(a). The critical state line (CSL) and the failure line (FL) obtained from drained triaxial tests on loose and dense Changi sand are also shown in Fig. 6(a). The slopes of the CSL and the FL are $M_{cs} = 1.35$ and $\eta_f = 1.63$, respectively (Chu et al. 2003; Wanatowski and Chu 2007).

As shown in Fig. 6(a), the specimen in Test IST01 was first sheared along a drained path from $p_c' = 150$ kPa to a stress ratio of $q/p' = 1.13$. After that the external loads, i.e., the axial load and the cell pressure, were maintained constant to conduct an instability check along a strain path of $d\varepsilon_v/d\varepsilon_1 = -0.67$. Under these conditions, instability occurred at point B and the axial strain and the pore-water pressure increased suddenly, as shown in Fig. 6(b). After occurrence of such instability, it was no longer possible to maintain the axial load constant, and thus the deviatoric stress dropped significantly, as can be seen in Fig. 6(a). Physically, it was observed that the specimen collapsed suddenly, i.e., pre-failure instability had occurred. This behaviour resembles the instability that occurs in loose sand under undrained conditions. This observation shows that dense sand, despite exhibiting strain hardening behaviour under an undrained condition, can become as vulnerable as loose sand when it is subjected to a dilative strain path.

It needs to be pointed out that the instability shown in Fig. 6 was not only due to the control of a negative strain increment ratio but also due to the stress state upon the instability check, as reported by Chu et al. (1993) and Chu & Leong (2001). Also, the observed instability was not due to strain localization or rate/time effect, as explained by Chu et al. (1993). This type of pre-failure instability can only occur when appropriate conditions are met (i.e. adequate strain increment ratio and stress state).

Another instability test IST02 was carried out to further investigate the behaviour of medium dense sand under dilatancy rate controlled conditions as well as the effect of effective stress ratio, $\eta = q/p'$, on the pre-failure instability of sand. The effective stress path of Test IST02 is shown in Fig. 7(a). The effective stress path of Test IST01 (see Fig. 6a) is also replotted in Fig. 7(a) as a dashed line. Test IST02 was conducted in a similar way to Test IST01 (see Fig. 6) except that the constant load test with $d\varepsilon_v/d\varepsilon_1 = -0.67$ was initiated at $\eta = 1.04$ (point A') in Test IST02 and $\eta = 1.13$ (point A) in Test IST01, as shown in Fig. 7(a).

From the axial strain and pore water pressure versus time curves of Test IST02 presented in Fig. 7(b), it can be seen that the axial strain and pore water pressure started to accelerate when the stress state moved from point A' to point B'. Thus, instability occurred at point B' in Test IST02. As can be seen from the effective stress path plotted in Fig. 7(a), the deviatoric stress in Test IST02 started to reduce significantly at point B', where the instability occurred, reaching the FL at the end of test. This decrease was accompanied by an acceleration in the axial strain of the specimen (Fig. 7b), which means large plastic strains developed at point B'. Thus, using the two points, B and B', at which instability occurred, the instability line for $d\varepsilon_v/d\varepsilon_1 = -0.67$ can be determined as shown in Fig. 7(a). The slope of the instability line obtained from Tests IST01 and IST02, $\eta_{IL} = 1.13$, is the same as the slope of the peak stress line determined from deformation-controlled strain path tests SP09, SP10 and SP11 with $d\varepsilon_v/d\varepsilon_1 = -0.67$, as shown in Fig. 5(b). Thus, the peak stress line obtained from the dilatancy rate controlled tests and the instability line obtained from the instability

tests are equivalent and the occurrence of pre-failure instability in load-controlled strain path tests can be predicted with the peak stress line obtained from the deformation-controlled strain path tests.

It should also be mentioned that, similar to Test IST01, after the onset of instability, the specimen in Test IST02 has collapsed. Therefore, the instability observed in Test IST02 is a runaway type similar to undrained instability of loose sand under undrained conditions. Once runaway instability is initiated, the pore water pressure and the axial strain rates increase dramatically and the soil specimen collapses almost instantly. In other words the runaway instability cannot be ceased (Chu et al. 2003; Wanatowski & Chu 2012).

The volumetric strain and void ratio changes measured in Test IST02 are shown in Fig. 7(c). It can be seen from the volumetric strain curve that very small dilative volumetric changes were measured in the specimen before point B'. As a result, the void ratio of the specimen increased very little during this stage of Test IST02, as shown in Fig. 7(c). Once instability occurred, significantly more volumetric dilation was measured. This means that pre-failure instability in Test IST02 did not occur due to change of relative density.

The comparison of the effective stress paths obtained from Tests IST01 and IST02, plotted in Fig. 7(a) also shows that the eventual occurrence of instability was not influenced by the change in effective stress ratio. However, an increase in the effective stress ratio reduces the time taken for instability to occur, as the initial stress state at which constant load test was initiated moves closer to the instability line. It should be pointed out, however, that the effective stress ratio, q/p' , has to be sufficiently high to induce instability, as discussed in detail in following section.

DISCUSSION

Although pre-failure instability does not occur for dense sand under undrained conditions, an undrained condition may not be necessary for instability to occur as a soil element in a slope could be subjected to conditions in which pore water pressure and volume can be changed

simultaneously. This condition can be modelled experimentally by strain paths with the strain increment ratio ($d\varepsilon_v/d\varepsilon_1$) controlled. When $d\varepsilon_v/d\varepsilon_1 > 0$ is imposed on dense sand, the pore water pressure will decrease and instability will not occur. However, when an adequate dilative $d\varepsilon_v/d\varepsilon_1$ is imposed, the pore water pressure will increase and instability becomes a possibility.

It needs to be pointed out that when sand of different void ratios is sheared under a drained condition, the volumetric strain behaviour will be different. If the sand is loose, the volumetric strain will be contractive. On the other hand, if the sand is dense, it will dilate. A drained test defines the volumetric strain response of sand to a zero pore water pressure change condition. In other words, in order to maintain the pore water pressure to be constant, the volume of the sand will have to change in the way as measured in a drained test. In a drained test, loose sand needs to contract, that is to discharge water, to maintain the pore water pressure to be constant. On the other hand, when volume change, i.e., water discharge, is not allowed in an undrained test, the pore water pressure will increase. As a consequence, the effective confining stress will decrease and the shear resistance will decrease accordingly. Static liquefaction or runaway instability will occur. Similarly, in a drained test, a dense sand needs to dilate, i.e., to absorb water, to maintain the pore water pressure to be constant. Under an undrained condition, water is not allowed to flow into the specimen and hence the pore water pressure inside the specimen will reduce. This is what is observed in an undrained test on dense sand. However, if a dilatancy rate controlled condition is imposed to force the specimen to dilate more than the sand would under a drained condition, extra water will have to flow into the specimen to generate the required dilation. As a result, positive pore water pressure will develop. The specimen will become unstable in a similar way as in an undrained test on loose sand.

The occurrence of runaway instability is affected by factors such as, the drainage conditions which can be simulated by the strain increment ratio imposed, $(d\varepsilon_v/d\varepsilon_1)_i$ the void ratio of soil, and the initial effective stress ratio. As discussed in detail by Chu et al. (1993), the instability condition for both loose and dense sand can be expressed by the differences between the strain increment ratio

imposed during a strain path test, $(d\varepsilon_v/d\varepsilon_1)_i$, and the strain increment ratio of the soil, $(d\varepsilon_v/d\varepsilon_1)_s$, measured in a drained test. Instability occurs when:

$$\left(\frac{d\varepsilon_v}{d\varepsilon_1}\right)_i - \left(\frac{d\varepsilon_v}{d\varepsilon_1}\right)_s \leq 0 \quad (2)$$

The strain increment ratio of the soil, $(d\varepsilon_v/d\varepsilon_1)_s$, is the maximum $d\varepsilon_v/d\varepsilon_1$ ratio determined from the ε_v - ε_1 curve of a drained test conducted under the same initial effective confining stress. For very loose sand, $(d\varepsilon_v/d\varepsilon_1)_s$ is greater than or equal to zero. Instability tends to occur when $(d\varepsilon_v/d\varepsilon_1)_i = 0$, i.e., under an undrained condition. For medium loose to dense sand, $(d\varepsilon_v/d\varepsilon_1)_s$ is negative. Instability is only possible when $(d\varepsilon_v/d\varepsilon_1)_i$ is even more negative than $(d\varepsilon_v/d\varepsilon_1)_s$.

Constitutive equations can be used to predict the value of $(d\varepsilon_v/d\varepsilon_1)_s$ in Inequality (2). If the modified Rowe's stress-dilatancy theory (Rowe 1962, Wan & Guo 1998) is used for a drained test, $(d\varepsilon_v/d\varepsilon_1)_s$ can be calculated as:

$$\left(\frac{d\varepsilon_v}{d\varepsilon_1}\right)_s = 1 - \frac{1}{K} \left(\frac{\sigma_1'}{\sigma_3'}\right)_f \quad (3)$$

where $(\sigma_1'/\sigma_3')_f$ = failure stress ratio achieved in a drained test, and K is expressed as:

$$K = \frac{1 + \sin \phi^*}{1 - \sin \phi^*} \quad \text{with} \quad \sin \phi^* = (e / e_{cr})^\alpha \sin \phi_{cr} \quad (4)$$

where ϕ^* is the friction angle mobilized along a certain macroscopic plane which evolves during deformation history, ϕ_{cr} and e_{cr} are the friction angle and void ratio at critical state, and α is a parameter to be determined from laboratory tests (Wan & Guo 1998).

Combining Eq. (3) with Inequality (2) leads to:

$$\left(\frac{d\varepsilon_v}{d\varepsilon_1}\right)_i \leq 1 - \frac{1}{K} \left(\frac{\sigma_1'}{\sigma_3'}\right)_f \quad (5)$$

Since $(\sigma_1'/\sigma_3')_f$ depends on the initial void ratio and to a certain extent on the effective confining stress, Inequality (5) reflects the influence of these two factors, in addition to $(d\varepsilon_v/d\varepsilon_1)_i$, on pre-failure instability.

As discussed earlier, the effect of stress ratio on the instability behaviour of loose sand under undrained conditions is specified by the instability line shown in Fig. 3. Similarly, the effect of void ratio on the instability behaviour of dense sand under dilatancy rate controlled conditions is specified by the peak stress line, as shown in Fig. 5(b). In both cases, the stress ratio, η , has to be sufficiently high to induce instability (Chu & Leong 2001). This can be explained by plasticity theory. For plastic flow to develop, the yield surface has to expand, which requires the stress increment to point outside the yield surface. A typical yield surface for sand is shown in Fig. 8. The effective stress path involved in an instability test is characterized by $dq \leq 0$ and $dp' < 0$. In instability tests the deviator stress q decreases because the cross-section of the specimen increases while the deviator load is maintained constant. The effective mean stress p' decreases due to the increase in pore pressure. As shown in Fig. 8, such a stress path only points outside the yield surface when it is within the hatched zone. In terms of stress state, this hatched zone has a stress ratio higher than the stress ratio at the peak point of the yield surface. If the stress ratio where an instability test starts is lower than the stress ratio at the peak point, such a stress path will point inside the yield surface, as shown in Fig. 8, and result in an elastic response. The hatched area is characterized by a negative normal direction. Mathematically, this can be expressed as:

$$\frac{\partial f}{\partial p'} < 0 \quad (6)$$

where f is the yield surface.

Inequality (6) defines the stress conditions under which instability may occur. These conditions are approximately defined by the instability line shown in Fig. 3 and the peak stress line shown in Fig. 5(b). Therefore, these lines are associated with the yield surface and define the conditions in which large plastic yielding can take place (Lade 1992; Chu et al. 1993; Imam et al. 2002; Chu et al. 2003). As such, the zone of instability can be defined for specific drainage conditions if appropriate strain increment ratio, $d\varepsilon_v/d\varepsilon_1$ is imposed to specimens. Therefore, pre-

failure instability can occur under various drainage conditions as long as the stress path leads the stress state into the zone of potential instability.

It should be pointed out that pre-failure instability investigated in this paper is defined as behaviour in which large plastic strains are generated rapidly. For large plastic strain to develop, the soil must be in a yielding state. Therefore, yielding is the necessary condition for instability. This has been explained by Lade (1992) for the instability occurring for loose sand under undrained conditions and Chu et al (2003), Wanatowski et al. (2010), and Chu et al. (2012) for the instability occurring for both loose and dense sand under drained conditions. The Instability Line, in fact, is defined based on the yielding conditions (Lade 1992; Chu et al. 1993, 2003). This explains why instability can occur under undrained, drained and dilatancy controlled conditions as long as the stress path leads the stress state into the zone of instability.

It is also important to note that although the condition given by Inequality (6) involves the yield surface, the conditions for the occurrence of pre-failure instability can be determined without establishing the exact yield function. When soil is sheared along a constant deviator stress path, yielding is not precisely defined by the Instability Line obtained by the line linking the peak points of the yield surfaces (Lade 1992, 1993; Chu et al. 2003). Nevertheless, the Instability Line defines the lower bound of all the possible unstable conditions for undrained and drained shearing. Similarly, the peak stress line can be used to determine all the possible unstable conditions under generalised drainage conditions simulated in the laboratory by controlling dilatancy rate. This is verified by the experimental data presented in this paper.

CONCLUSIONS

Several triaxial tests were carried out to study pre-failure instability of sand under dilatancy rate controlled conditions. The following conclusions can be derived from this study:

1. Pre-failure instability does not need to occur under undrained conditions. The testing data presented in this paper have shown that instability can occur under a dilatancy rate

controlled condition, that is when the soil is dilating. Whether a soil element will undergo instability depends on the difference between the strain increment ratio of the soil obtained from a drained test, $(d\varepsilon_v/d\varepsilon_1)_s$, and the strain increment ratio imposed during the strain path test, $(d\varepsilon_v/d\varepsilon_1)_i$, rather than the absolute magnitude of $(d\varepsilon_v/d\varepsilon_1)_s$.

2. From a series of dilative strain path tests conducted at different effective confining pressures with the same $d\varepsilon_v/d\varepsilon_1$ a peak stress line can be determined by joining the peak points of the effective stress paths to the origin in the q - p' stress space. This is similar to define the instability line from undrained tests.
3. The instability tests under dilatancy rate controlled conditions indicate that the stress ratio at the onset of instability η_{IL} obtained in the instability tests coincides with that of the peak stress line η_p . This means that the peak stress line can be used to predict the onset of instability of medium loose to dense sand under dilatancy rate controlled conditions in a way similar to the use of instability line for loose sand under undrained conditions.
4. The conditions for the occurrence of pre-failure instability are defined based on the yielding conditions. Thus, the zone of instability can be determined regardless of the drainage conditions. However, the occurrence of pre-failure instability can be predicted without establishing the yield function if the method described in this paper is used.

REFERENCES

- Adalier, K. & Elgamal, A.-W. (2002). Seismic response of adjacent dense and loose saturated sand columns. *Soil Dyn. Earth. Engng* 22, 115-127.
- Andrade, J. E. (2009). A predictive framework for liquefaction instability. *Géotechnique* 59, No. 8, 673-682.

- Been, K., Conlin, B. H., Crooks, J. H. A., Fitzpatrick, S. W., Jefferies, M. G., Rogers, B. T. & Shinde, S. (1987). Back analysis of the Nerlerk berm liquefaction slides: discussion. *Can. Geotech. J.* 24, 170-179.
- Been, K., Crooks, J. H. A., Conlin, B. H. & Horsfield, D. (1988). Liquefaction of hydraulically placed sand fills. In *Hydraulic Fill Structures, ASCE Geotechnical Special Publication 21*, (eds D. J. A. Van Zyl and S. G. Vick), pp. 573-591.
- Casagrande, A. (1936). Characteristics of cohesionless soils affecting the stability of earth fills. In *Contributions to Soil Mechanics: 1925-1940*. Boston Society of Civil Engineers, pp. 257-276.
- Chu, J. & Leong, W. K. (2001). Pre-failure strain softening and pre-failure instability of sand: a comparative study. *Géotechnique* 51, No. 4, 311-321.
- Chu, J. & Lo, S.-C. R. (1991). On the implementation of strain path testing. In *Proc. 10th Eur. Conf. Soil Mech.*, Florence, pp. 53-56.
- Chu, J. & Wanatowski, D. (2009). Effect of loading mode on strain softening and instability behavior of sand in plane-strain tests. *J. Geotech. Geoenviron. Engng ASCE* 135, No. 1, 108-120.
- Chu, J., Lo, S.-C. R. & Lee, I. K. (1992). Strain-softening behaviour of a granular soil in strain-path testing. *J. Geotech. Engng ASCE* 118, No. 2, 191-208
- Chu, J., Lo, S.-C. R. & Lee, I. K. (1993). Instability of granular soils under strain path testing. *J. Geotech. Engng ASCE* 119, No. 5, 874-892.
- Chu, J., Leroueil, S. & Leong, W. K. (2003). Unstable behaviour of sand and its implication for slope stability. *Can. Geotech. J.* 40, 873-885.
- Chu, J., Leong, W.K., Loke, W.L. & Wanatowski, D. (2012), Instability of loose sand under drained conditions, *J. Geotech. Geoenviron. Engng ASCE* 138, No. 2, 207-216.
- Eckersley, J. D. (1990). Instrumented laboratory flowslides. *Géotechnique* 40, 489-502.

- Fleming, R. W., Ellen, S. D. & Albus, M. A. (1989). Transformation of dilative and contractive landslide debris into debris flows - An example from Marin County, California. *Engng Geol.* 27, 201-223.
- Hadala, P. F. & Torrey, V. H. (1989). Mississippi riverbank flowslides. In *The Art and Science of Geotechnical Engineering*, Prentice-Hall Inc., Englewood Cliffs., N.J., pp. 13-30.
- Imam, S. M. R., Morgenstern, N. R., Robertson, P. K. & Chan, D. H. (2002). Yielding and flow liquefaction of loose sand. *Soils Found.* 42, No. 3, 19-31.
- Kokusho, T. (2003). Current state of research on flow failure considering void redistribution in liquefied deposits. *Soil Dyn. Earth. Engng* 23, 585-603.
- Lade, P. V. (1992). Static instability and liquefaction of loose fine sandy slopes. *J. Geotech. Engng ASCE* 118, No. 1, 51-72.
- Lade, P. V. (1993). Initiation of static instability in the submarine Nerlerk berm. *Can. Geotech. J.* 30, 895-904.
- Lade, P. V. & Pradel, D. (1990). Instability and plastic flow of soils. I: Experimental observations. *J. Engng Mech.* 116, No. 11, 2532-2550.
- Lancelot, L., Shahrour, I. & Al Mahmoud, M. (2004). Instability and static liquefaction on proportional strain paths for sand at low stresses. *J. Engng Mech.* 130, No. 11, 1365-1372.
- Leong, W. K., Chu, J. & Teh, C. I. (2000). Liquefaction and instability of a granular fill material. *Geotech. Test. J. ASTM* 23, No. 2, 178-192.
- Lo, S.-C. R., Chu, J. & Lee, I. K. (1989). A technique for reducing membrane penetration and bedding errors. *Geotech. Test. J. ASTM* 12, No.4, 311-316.
- National Research Council (1985). *Liquefaction of soils during earthquakes*. Washington, DC: National Academy Press.
- Olson, S. M., Stark, T. D., Walton, W. H. & Castro, G. (2000). 1907 static liquefaction flow failure of the north dike of Wachusett dam. *J. Geotech. Geoenviron. Engng ASCE* 126, No. 12, 1184-1193.

- Rowe, P. W. (1962). The stress dilatancy relationship for static equilibrium of an assembly of particles in contact. *Proc. Royal Society A*269, 500-527
- Rowe, P. W. & Barden, L. (1964). Importance of free ends in triaxial testing. *J. Soil Mech. Found. Div. ASCE* 90, No. 1, 1-15.
- Sasitharan, S., Robertson, P. K., Sego, D. C. & Morgenstern, N. R. (1993). Collapse behavior of sand. *Can. Geotech. J.* 30, No. 4, 569-577.
- Schofield, A. N. (1980). Cambridge geotechnical centrifuge operations. *Géotechnique* 30, No. 3, 227-268.
- Sento, N., Kazama, M., Uzuoka, R., Ohmura, H. & Ishimaru, M. (2004). Possibility of postliquefaction flow failure due to seepage. *J. Geotech. Geoenviron. Engng ASCE* 129, No. 8, 727-737.
- Sivathayalan, S. & Logeswaran, P. (2007). Behaviour of sands under generalized drainage conditions, *Can. Geotech. J.* 44, 138-150.
- Sladen, J. A., D'Hollander, R. D. & Krahn, J. (1985). The liquefaction of sands, a collapse surface approach. *Can. Geotech. J.* 22, 564-578.
- Topolnicki, M., Gudehus, G. & Mazurkiewicz, B. K. (1990), Observed stress-strain behaviour of remoulded saturated clay under plane-strain conditions. *Géotechnique* 42, No. 2, 155-187.
- Torrey, V. H. & Weaver, F. J. (1984). Flow failures in Mississippi riverbanks. In *Proc. 3rd Int. Symposium on Landslides*, Toronto, 2, 335-360.
- Vaid, Y. P. & Eliadorani, A. (1998): Instability and liquefaction of granular soils under undrained and partially drained states. *Can. Geotech. J.* 35, 1053-1062.
- Wan, R. G. & Guo, P. J. (1998). A simple constitutive model for granular soils: modified stress-dilatancy approach. *Comp. Geotech.* 22, 109-133.
- Wanatowski, D. & Chu, J. (2007). Static liquefaction of sand in plane-strain. *Can. Geotech. J.* 44, 299-313.

- Wanatowski, D., Chu, J., & Lo, R. S.-C. (2008), Strain softening behaviour of sand in strain path testing under plane-strain conditions, *Acta Geotech.* 3, No. 2, 99-114.
- Wanatowski, D., Chu, J., and Loke, W. L. (2010), Drained instability of sand in plane-strain, *Can. Geotech. J.* 47, No. 4, 400-412.
- Wanatowski, D., & Chu, J. (2011), Pre-failure instability behavior of sand in strain path testing under plane-strain conditions, *Soils and Foundations* 51, No. 3, 423-435.
- Wanatowski, D. & Chu, J. (2012). Factors affecting pre-failure instability of sand under plane-strain conditions, *Géotechnique* 62, No.2, 121-135
- Yang, J. (2002). Non-uniqueness of flow liquefaction line for loose sand. *Géotechnique* 52, No.10, 757-760.

List of figures

- Fig. 1.** Failure mechanisms identified by the U.S. National Research Council: (a) Mechanism B for the situation where void redistributes within a globally undrained sand layer; (b) Mechanism C for the situation where failure is induced by spreading of excess pore pressure with global volume changes.
- Fig. 2.** Typical behaviour of loose and dense sand under undrained conditions: (a) stress-strain curves; (b) effective stress paths.
- Fig. 3.** The critical state line, the instability line and the zone of potential instability defined by drained and undrained triaxial tests conducted on loose sand.
- Fig. 4.** Comparison of dilative and undrained strain paths of medium dense sand: (a) stress-strain behaviour; (b) effective stress paths; (c) excess pore water pressure curves.
- Fig. 5.** Results of $d\varepsilon_v/d\varepsilon_1 = -0.67$ strain path tests: (a) stress-strain curves; (b) effective stress paths; (c) excess pore water pressure curves.
- Fig. 6.** Results of Test IST01: (a) effective stress path; (b) axial strain and excess pore water pressure versus time curves.
- Fig. 7.** Results of Test IST02: (a) effective stress paths; (b) axial strain and pore water pressure versus time curves (c) volumetric strain and void ratio versus time curves.
- Fig. 8.** Yielding as a condition for instability.

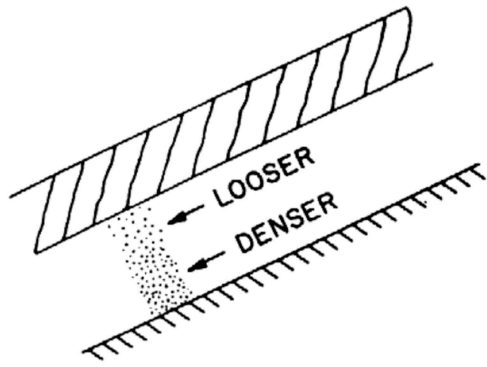


Fig. 1(a)

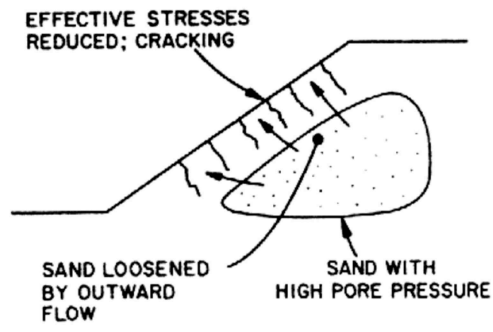


Fig. 1(b)

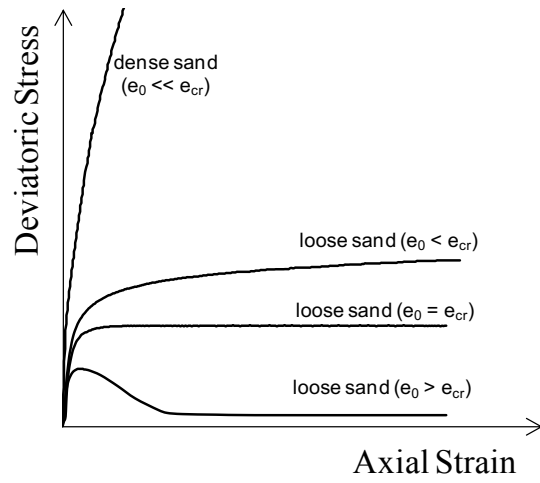


Fig. 2(a)

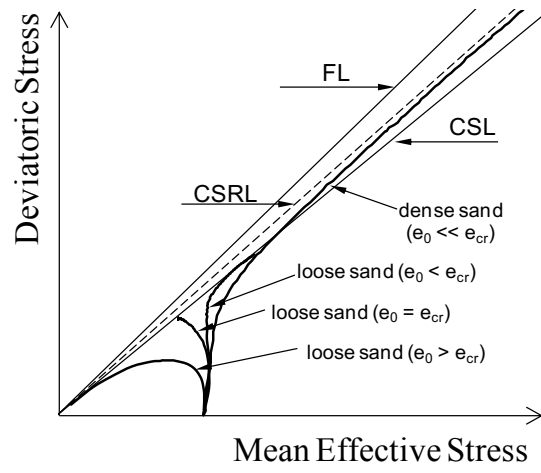


Fig. 2(b)

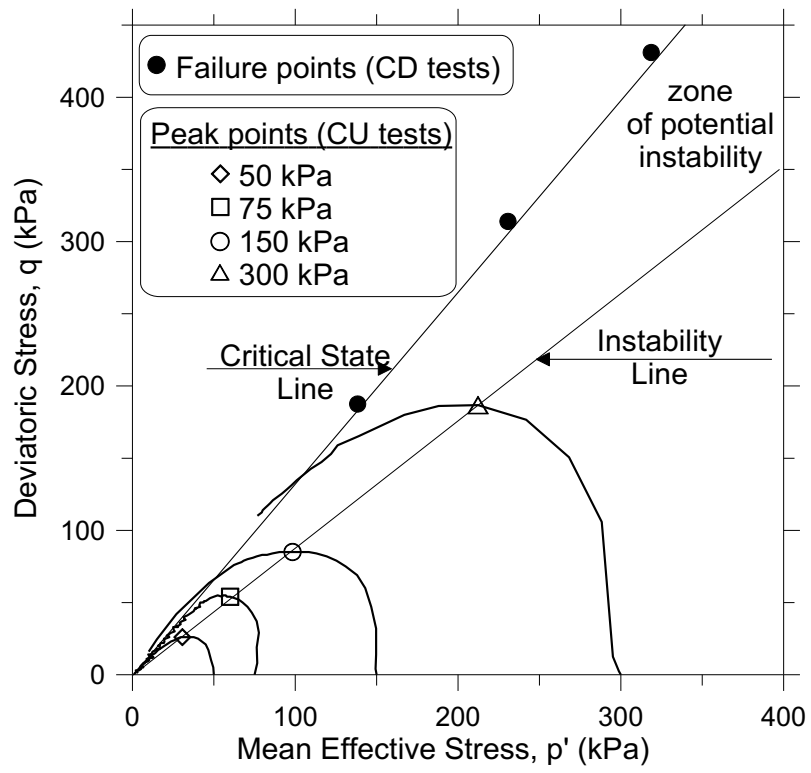


Fig. 3

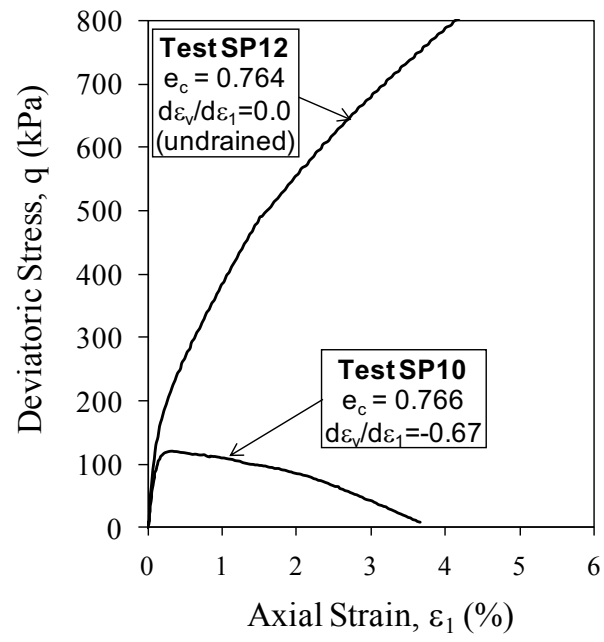


Fig. 4(a)

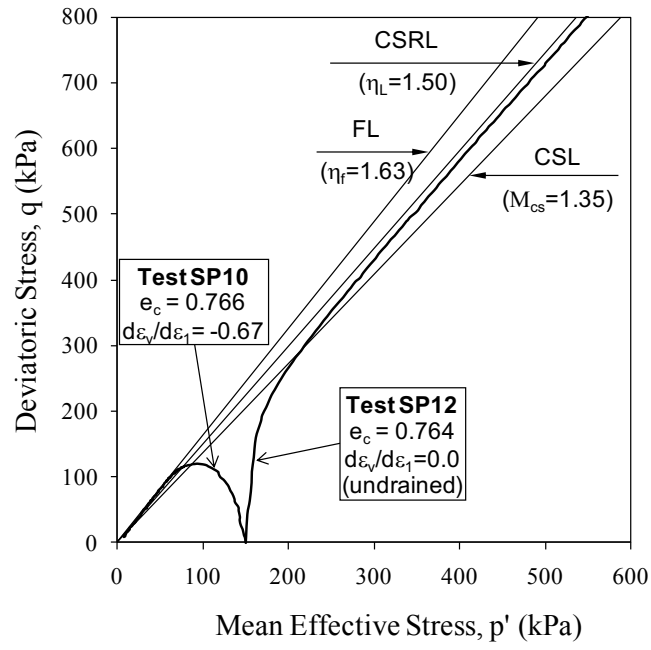


Fig. 4(b)

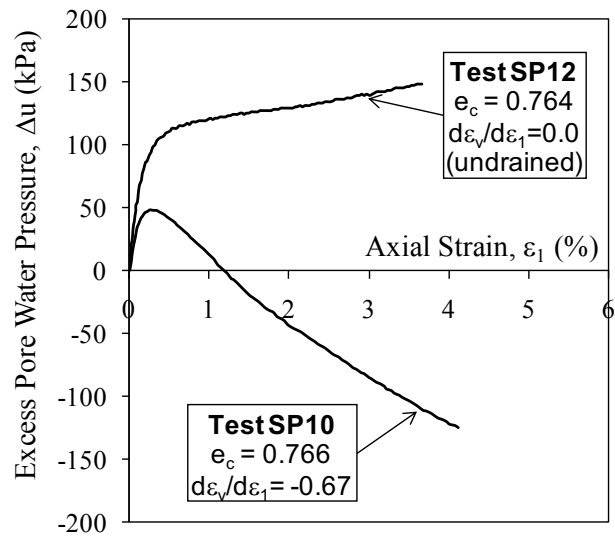


Fig. 4(c)

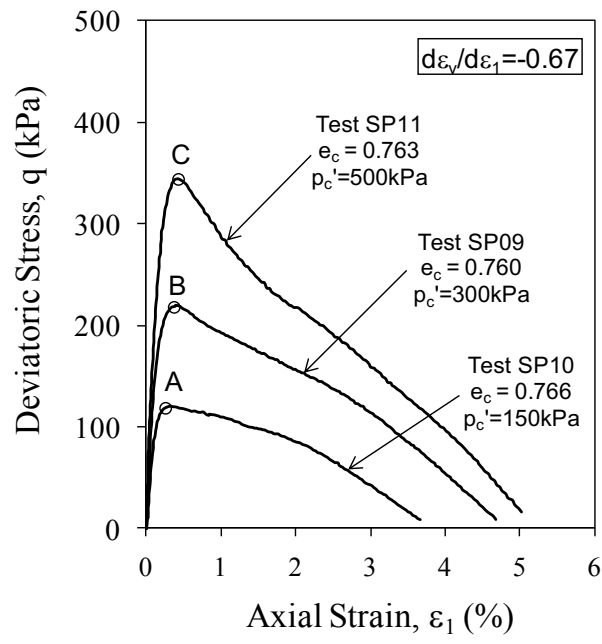


Fig. 5(a)

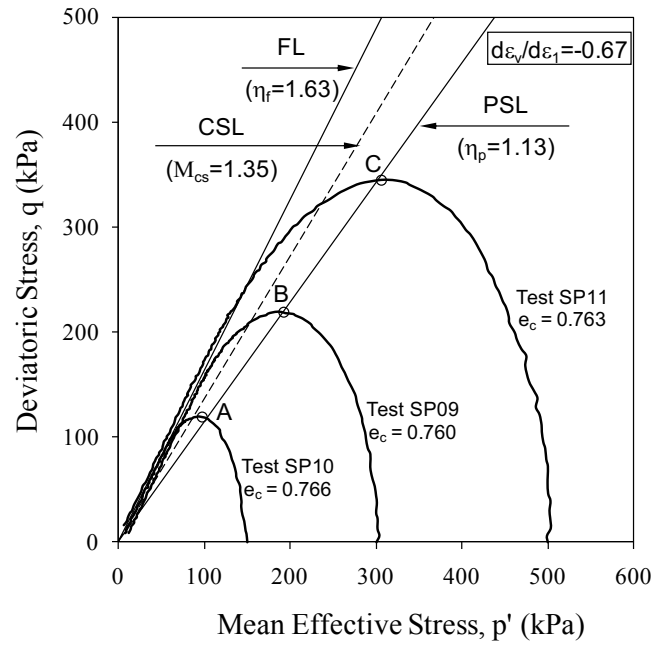


Fig. 5(b)

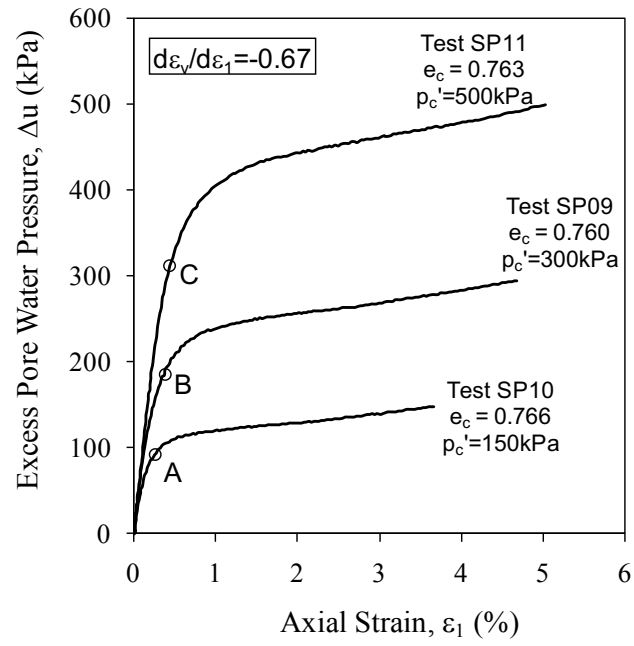


Fig. 5(c)

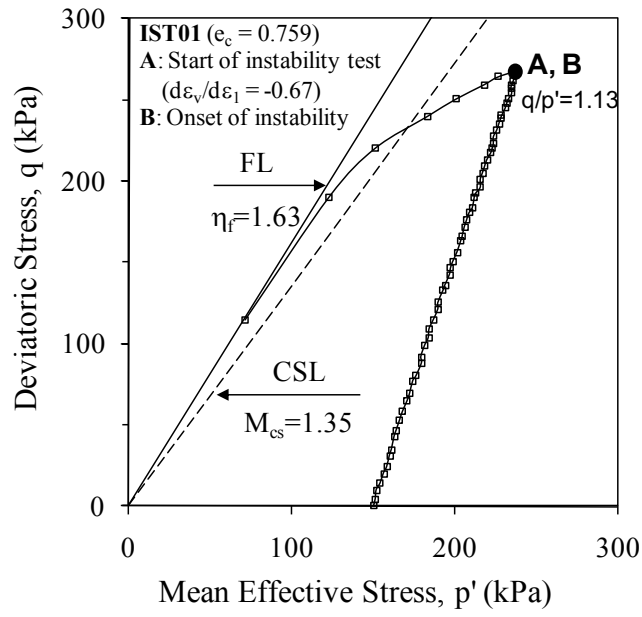


Fig. 6(a)

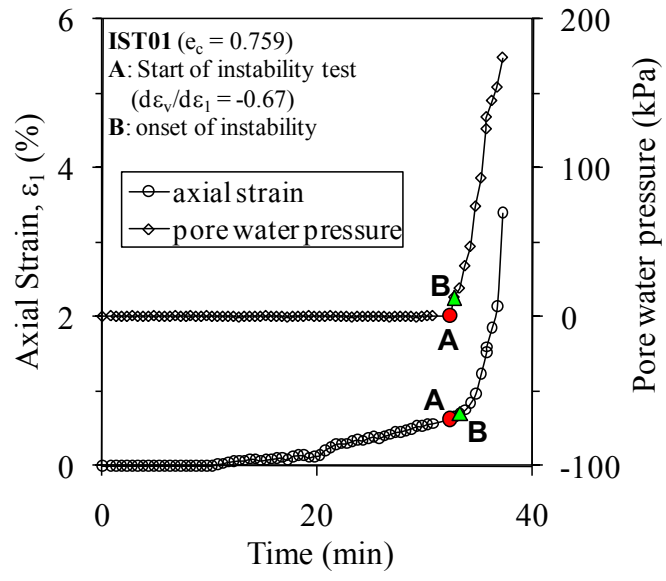


Fig. 6(b)

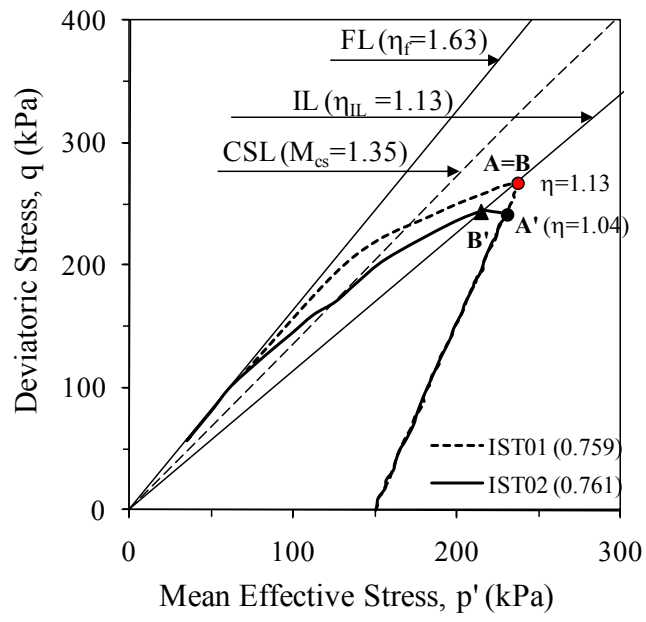


Fig. 7(a)

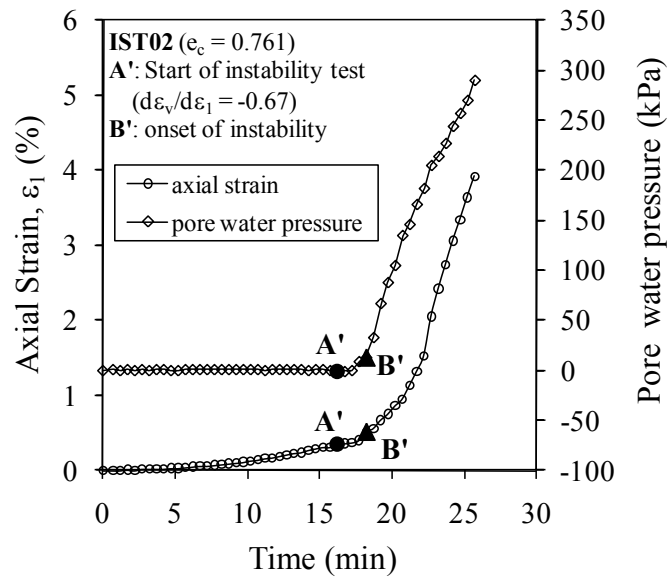


Fig. 7(b)

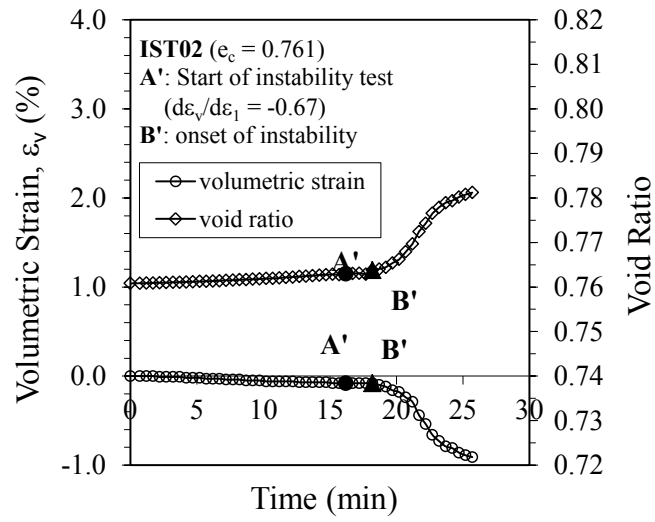


Fig. 7(c)

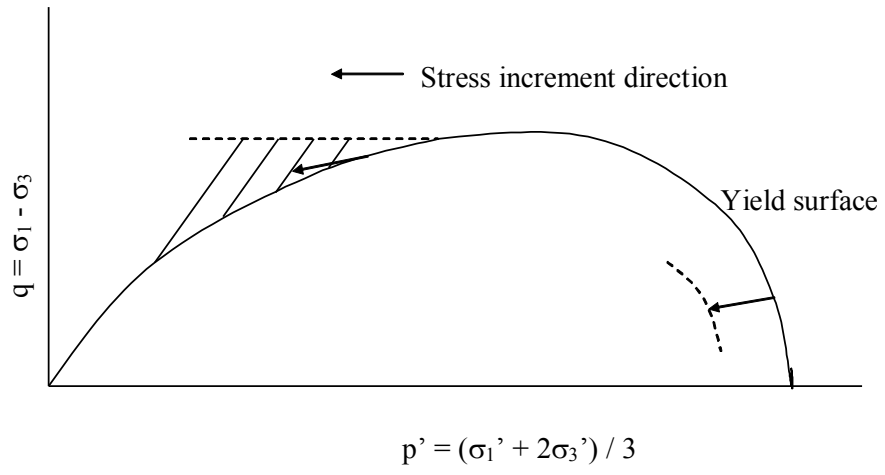


Fig. 8

Table 1. Basic properties of the tested sand.

Mean grain size (mm)	Uniformity coefficient	Specific gravity	Max. void ratio	Min. void ratio	Shell content (%)
0.30	2.0	2.60	0.916	0.533	12